



# Understanding the Land Carbon Cycle with Space Data: Current Status and Prospects

Jean-François Exbrayat<sup>1</sup> · A. Anthony Bloom<sup>2</sup> · Nuno Carvalhais<sup>3,6</sup> · Rico Fischer<sup>4</sup> · Andreas Huth<sup>4,7,8</sup> · Natasha MacBean<sup>5</sup> · Mathew Williams<sup>1</sup>

Received: 20 July 2018 / Accepted: 7 January 2019 / Published online: 6 February 2019  
© Springer Nature B.V. 2019

## Abstract

Our understanding of the terrestrial carbon cycle has been greatly enhanced since satellite observations of the land surface started. The advantage of remote sensing is that it provides wall-to-wall observations including in regions where in situ monitoring is challenging. This paper reviews how satellite observations of the biosphere have helped improve our understanding of the terrestrial carbon cycle. First, it details how remotely sensed information of the land surface has provided new means to monitor vegetation dynamics and estimate carbon fluxes and stocks. Second, we present examples of studies which have used satellite products to evaluate and improve simulations from global vegetation models. Third, we focus on model data integration approaches ranging from bottom-up extrapolation of single variables to carbon cycle data assimilation system able to ingest multiple types of observations. Finally, we present an overview of upcoming satellite missions which are likely to further improve our understanding of the terrestrial carbon cycle and its response to climate change and extremes.

**Keywords** Terrestrial carbon cycle · Earth observation · Satellite · Ecosystem modelling · Model data integration

## 1 Introduction

Terrestrial ecosystems help offset climate change by absorbing 25–30% of anthropogenic emissions of carbon dioxide (CO<sub>2</sub>) each year (Canadell et al. 2007; Le Quéré et al. 2018). The global land carbon sink is calculated as the residual between reported fossil-fuel emissions, measurements of the atmospheric CO<sub>2</sub> growth and constrained estimates of ocean carbon uptake (see, for example, Le Quéré et al. 2018 for more details). The spatio-temporal distribution of the land carbon sink is estimated using an ensemble of process-based terrestrial ecosystem models (TEMs; Sitch et al. 2015). However, these largely unconstrained models exhibit significant differences in the location, magnitude and sign of the land carbon balance. This lack of agreement leads to large uncertainties in Earth system models'

---

✉ Jean-François Exbrayat  
[j.exbrayat@ed.ac.uk](mailto:j.exbrayat@ed.ac.uk)

Extended author information available on the last page of the article

projections of the response of terrestrial ecosystems to future climate change (Friedlingstein et al. 2006; Arora et al. 2013). This is further complicated by the interplay of vegetation CO<sub>2</sub> uptake and emissions from land use and land cover change (Arneth et al. 2017) such as deforestation (van der Werf et al. 2009).

A key issue for TEMs has been the challenge of integrating global observations to calibrate process parameters. Model spread seems to emerge from the lack of understanding of processes that control carbon allocation, turnover and mortality (Friend et al. 2014). Although networks of eddy covariance towers (e.g., FLUXNET, Baldocchi et al. 2001) provide useful information to improve models (Williams et al. 2009; Kuppel et al. 2014), their distribution is highly skewed towards temperate regions of the Northern Hemisphere which challenges their applicability to other ecosystems. However, in recent years the multiplication of continuous Earth Observation (EO) has allowed the production of observational datasets relevant to the biosphere. While satellites do not measure carbon stocks and fluxes directly, they provide covariates for the extrapolation of in situ data to global gridded products related to ecosystem carbon fluxes (e.g., Jung et al. 2009) and biomass stocks (e.g., Saatchi et al. 2011; Baccini et al. 2012; Avitabile et al. 2016) through machine learning. Integrating EO to constrain process-based models has led to breakthrough in our understanding of the terrestrial carbon cycle, allowing a robust attribution of the increasing atmospheric CO<sub>2</sub> amplitude to the response of high latitude productivity (Forkel et al. 2016).

In this paper, we review studies in which satellite-driven datasets have been used to improve our understanding of the terrestrial carbon cycle. We first focus on studies in which EO products have been used to monitor vegetation dynamics, carbon fluxes and stocks. Then, we illustrate how EO products can be used to evaluate TEMs, understand their biases and improve projections of the carbon cycle. Third, we present model data integration approaches in which EO products are used to constrain TEMs using automated model data fusion approaches. Finally, we review the foreseeable improvements future satellite missions are likely to generate.

## 2 Earth Observation to Monitor Vegetation Dynamics, Carbon Fluxes and Stocks

Satellite observations of the land surface allow a continuous monitoring of vegetation dynamics through the calculation of spectral indices (Myneni et al. 1995). One of the most common metrics is the Normalized Difference Vegetation Index (NDVI). It is calculated such as  $NDVI = (NIR + RED) / (NIR - RED)$  where RED and NIR are the spectral reflectance in the visible red and near-infrared region of the photosynthetically active radiation spectrum, respectively. Because chlorophyll strongly absorbs visible light during photosynthesis, active canopies have higher NDVI values.

NDVI has been used in numerous studies to characterize the response of plant phenology and productivity to climate trends and inter-annual variability. Bimonthly NDVI from the Advanced Very High-Resolution Radiometer (AVHRR), supported by the National Oceanic and Atmospheric Administration (NOAA), spans the period since July 1981 until present. This long-term dataset has allowed describing a lengthening of the growing season in temperate regions of the Northern Hemisphere due to an earlier disappearance of snow in warming conditions (Myneni et al. 1997). Using the third generation of the AVHRR-based Global Inventory Modelling and Mapping System (GIMMS) NDVI dataset (Pinzon

and Tucker 2014), Buitenwerf et al. (2015) detected significant changes in phenological cycles for more than half of the land surface between 1981 and 2012. This long-term dataset has also been used to identify dominant climate modes driving the inter-annual variability in the start of growing season across North America (Dannenberg et al. 2018).

Higher-resolution NDVI data from the Moderate Resolution Imaging Spectroradiometer (MODIS) sensor (Huete et al. 2002) have been provided by the National Aeronautics and Space Administration (NASA) since the year 2000. These data have been used to attribute the anomalous greening of the Northern Hemisphere land surface in 2015 to a strong state of the Pacific Decadal Oscillation (Bastos et al. 2017). The MODIS archive also includes an Enhanced Vegetation Index (EVI) which performs well better in high biomass regions (Huete et al. 2002). It has been used to describe leaf growth across the Amazon basin during the dry season, which promotes primary productivity in sunnier conditions (Huete et al. 2006). EVI has also been used to describe the phenological response of Australian ecosystems to climate IAV (Broich et al. 2014), in particular the continental greening that followed the extremely wet 2010/11 La Niña episode (Fasullo et al. 2013).

NDVI and EVI are useful proxies for vegetation activity, but they are not biophysical variables directly relatable to TEMs. However, two key state variables for these models can also be derived from EO: the Fraction of Absorbed Photosynthetically Active Radiation (FAPAR) and Leaf Area Index (LAI), the one-sided area of leaves per units of ground. FAPAR and LAI are related to NDVI (Zhu et al. 2013) but can also be retrieved using physically based (Knyazikhin et al. 1998) or machine learning (Baret et al. 2013) methods.

FAPAR is a key driver for light use efficiency models of primary productivity (e.g., Potter et al. 1993; Field et al. 1995; Prince and Goward 1995; Knorr 2000). Global MODIS-based FAPAR (Myneni et al. 2002) is used to produce high-resolution (~1 km) estimates of gross primary productivity (GPP) and net primary productivity (NPP) across the global land surface (Running et al. 2004). This dataset has provided insights in a possible reduction in global net primary productivity because of a drying in the Southern Hemisphere (Zhao and Running 2010). It helped characterized the influence of the El Niño—Southern Oscillation on regional and global NPP (Bastos et al. 2013) and the impact of recent European heat waves on productivity (Bastos et al. 2014).

LAI represents the physiologically active part of the vegetation which interacts with the atmosphere and is a key state variable for land surface and ecosystem models (Kala et al. 2014). Figure 1 presents mean annual LAI for the year 2015 derived from the European Space Agency (ESA)'s Proba-V satellite (Baret et al. 2013) as part of the European Union's Copernicus programme and from NASA's MODIS sensor. There is a good agreement in the spatial distribution of LAI between these datasets, but the MODIS products report higher LAI values for tropical which may lead to non-negligible differences in the calculation of energy, water and carbon fluxes (Kala et al. 2014). MODIS LAI data have been helpful to understand the seasonality of the Amazon (Myneni et al. 2007). Zhu et al. (2013) used the relationship between AVHRR NDVI and MODIS FAPAR and LAI products to create the GIMMS FAPAR3 g and LAI3 g dataset extending back to the 1980s. This long-term dataset exhibits a greening trend, i.e. an increase in LAI during the growing season (Zhu et al. 2016).

A recent advance in remote sensing has been the production of solar-induced fluorescence (SIF) retrievals (Frankenberg et al. 2011). SIF is directly related to plant photosynthetic activity; therefore, SIF data provide a more direct measure of gross C uptake than reflectance-based indicators like NDVI or FAPAR (Porcar-Castell et al. 2014). There has been an increase in the availability of global SIF products derived from space-borne instruments like GOSAT, developed by the Japan Aerospace Exploration Agency (JAXA),

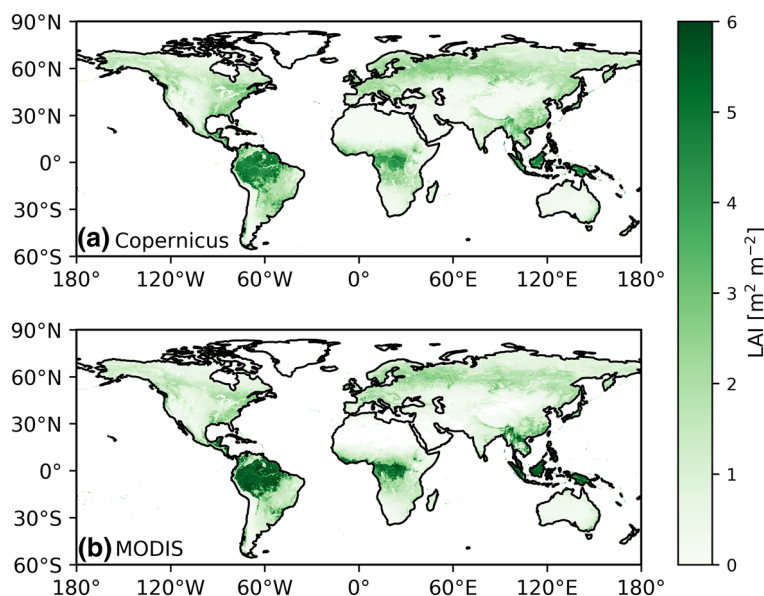


**Fig. 1** Mean Leaf Area Index (LAI) in 2015 according to **a** Copernicus and **b** NASA's MODIS. Datasets were resampled at 0.25° spatial resolution for plotting purposes

(Frankenberg et al. 2011; Guanter et al. 2012), GOME-2, designed by the German Aerospace Centre (DLR) (Joiner et al. 2013; Köhler et al. 2015), SCIAMACHY from ESA (Joiner et al. 2016) and OCO-2 from NASA (Sun et al. 2018). More details about SIF are provided in Sect. 3.2.3 of the review by Scholze et al. (2017).

Additionally to plant productivity, satellite datasets have been used for over three decades to monitor fire, a fundamental component of the terrestrial carbon cycle which accounts for a large degree of the inter-annual variability of the terrestrial land sink (van der Werf et al. 2010; Le Quéré et al. 2018). Observations of decadal trends in burned area (Flannigan and Haar 1986; Giglio et al. 2013; Andela et al. 2017) have been used to establish the role of fires as a key component of the long-term C balance evolution (Le Quéré et al. 2018; Arora and Melton 2018, amongst others). A range of satellite-based observations of fire have also radically advanced insight into continental-scale fire characteristics and processes, including understory fires (Morton et al. 2013); fire radiative power (Freeborn et al. 2014); and interactions between fire and species distribution (Rogers et al. 2015). Archibald et al. (2013) identified 5 dominant types of fire regimes using remotely sensed observation of fire frequency, radiative power and size. Active fire detection also offers a crucial constraint on land C fire losses, with current observing system such as VIIRS offering new possibilities to detect boreal fires (Waigl et al. 2017).

Beyond monitoring vegetation dynamics and inferring land-atmosphere fluxes, satellite observations have allowed the creation of high-resolution maps of above-ground biomass (AGB) covering large regions such as the pantropics (e.g., Saatchi et al. 2011; Baccini et al. 2012). Pantropical maps were created using allometric equations (e.g., Chave et al. 2014) relating tree height measured by NASA's Geoscience Laser Altimeter System sensor onboard the Ice, Cloud and land Elevation Satellite (Zwally et al. 2002) to AGB. These wall-to-wall maps allow a first-order approximation of remotely sensed deforestation (e.g.,

Hansen et al. 2013) on AGB stocks in the tropics (Harris et al. 2012; Baccini et al. 2012). Recently, maps by Saatchi et al. (2011) and Baccini et al. (2012) have been fused with additional in situ measurements to create a third map, currently considered as the state of the art (Avitabile et al. 2016).

Thurner et al. (2014) created a map for the northern boreal and temperate forests paper using retrievals of Growing Stock Volume from Envisat Advanced Synthetic Aperture Radar (Santoro et al. 2011, 2015), database information about wood density (Chave et al. 2009) and allometric equations. Thurner et al. (2016) used this map in combination with MODIS NPP to evaluate gradients in turnover dynamics across these regions.

While these previous studies relied on a single AGB map to produce estimates of gross emissions from deforestation, more recent studies have produced annually resolved AGB maps which allow tracking the counteracting impact of regrowth and derive net changes of biomass globally. For example, Liu et al. (2015) used the correlation between Vegetation Optical Depth and AGB from Saatchi et al. (2011) to produce annual biomass maps for 1993–2012 at a 0.25° spatial resolution. They concluded to a loss of global AGB driven by a loss of tropical forests partially compensated by gains over boreal, temperate and savannah regions. More recently, Brandt et al. (2018) used a similar approach to describe a net carbon loss across sub-Saharan Africa for the period 2010–2016. Baccini et al. (2017) also concluded that the tropics are a net source of atmospheric CO<sub>2</sub> based on annual maps they constructed from 2003 to 2014.

EO is useful to identify land cover change (e.g., Hansen et al. 2013) and, by extension, intact forest landscapes (Potapov et al. 2008). Potential AGB maps, representative of the hypothetical undisturbed landscape, can be reconstructed using the relationship between AGB (Saatchi et al. 2011; Baccini et al. 2012; Liu et al. 2015) and climate (New et al. 2002) in these intact regions. This approach attributes ~1.5% of the recent increase in atmospheric CO<sub>2</sub> to the Amazonian deforestation (Exbrayat and Williams 2015) while climate change has reduced the capacity of these forests to recover (Exbrayat et al. 2017).

International policy efforts such as the Paris agreement on climate change and the Bonn challenge for forest restoration have raised the interest of countries to produce country-scale maps for monitoring and reporting. For example, Rodríguez-Veiga et al. (2016) used local information from the Mexican forestry. Similarly, Xu et al. (2017) produced a biomass map for the Democratic Republic of Congo using additional data which were not available to pantropical maps. Both studies presented measurable increase in mapping quality and uncertainty quantification.

### 3 Evaluating Terrestrial Ecosystem Models

Land surface models are key components of Earth system models that simulate energy and mass transfers between the land and the atmosphere; hence, these are key components in the prediction of climate variations from short to long time scales (Pitman 2003). EO of the biosphere provides unprecedented means to evaluate vegetation dynamics, carbon fluxes and biomass stocks simulated by land surface models in a temporally and spatially explicit manner. The evaluation strategies have been largely focusing on aspects related to: the timing of seasonal vegetation development and long-term trends in vegetation greenness; the seasonal and spatial variations in photosynthesis patterns; the spatial variations in plant carbon stocks; and EO-derived estimates of carbon turnover times on land.

The representation of phenology in land surface models is a major source of uncertainty for the calculation of energy, water and carbon fluxes (Kala et al. 2014). Many studies have focused on in situ evaluation of modelled LAI (e.g., Richardson et al. 2012; Migliavacca et al. 2012), but long-term EO-derived products have also been used. Zhu et al. (2013) described a systematic overestimation of LAI by 18 Earth system models compared to the GIMMS LAI3 g dataset. This was accompanied by a shift towards earlier peak in LAI in boreal regions. Similarly, Anav et al. (2013) evaluated models participating in the fifth phase of the Coupled Model Intercomparison Project (CMIP5; Taylor et al. 2012) which underpinned the fifth Assessment Report of the Intergovernmental Panel on Climate Change. They described a tendency for CMIP5 models to overestimate LAI, although most models captured LAI trends. The poor performance of models to represent phenology has led several inter-comparison projects to impose EO-derived LAI dataset to all participating models (Huntzinger et al. 2013; Haarsma et al. 2016).

EO-derived products have also been used to assess vegetation productivity simulated by ecosystem models. Kolby Smith et al. (2016) created a long-term NPP dataset based on MODIS NPP algorithm (Running et al. 2004; Zhao and Running 2010) driven by long-term GIMMS FAPAR3g (Zhu et al. 2013). They compared this new dataset with five CMIP5 models which exhibited a much stronger trend of increasing NPP than the EO-based product. They concluded that models' sensitivity to increasing atmospheric CO<sub>2</sub> was too high, probably owing to the lack of representation of nutrient limitation on productivity. Ito et al. (2017) showed that spatial and seasonal variations in GPP simulated by eight ecosystem models were in agreement with the MODIS GPP product. However, they also showed that models failed to simulate GPP anomalies in response to extreme events such as the 1997–1998 El Niño or the eruption of Mount Pinatubo in 1991. Slevin et al. (2017) identified an underestimation of GPP in the tropics when comparing the Joint UK Land Environment Simulator (JULES; Clark et al. 2011) with EO-derived GPP products.

EO-derived products of GPP and NPP now allow skill-based ensemble averaging studies to be applied to ecosystem models. These post-processing procedures have been used in atmospheric sciences for many decades (e.g., Krishnamurti et al. 1999) and can be applied to ecosystem models in a spatially explicit way. Schwalm et al. (2015) applied the Reliability Ensemble Averaging method (Giorgi and Mearns 2002) constrained by FLUXNET MTE-GPP and biomass estimates to ten ecosystem models participating to the MsTMIP (Huntzinger et al. 2013). Exbrayat et al. (2018a) used a similar method to constrain projections of twenty-first-century change in NPP predicted by 30 simulations from the ISIMIP ensemble (Friend et al. 2014; Warszawski et al. 2014). They showed that the uncertainty in global change in NPP could be reduced by two-thirds using a skill-based ensemble averaging while gaining confidence on the sign of the change for more than 80% of the global land surface.

A recent emphasis has been put on the need to move beyond the separate evaluation of pools and fluxes by terrestrial land models. For many years, global models have been initialized using a spin-up procedure from which biomass stocks would emerge as a result of input fluxes and turnover times at steady state (Exbrayat et al. 2014). However, models perform poorly to simulate vegetation carbon stocks in agreement with observation-based products. For example, Fig. 2 presents a comparison of the recent pantropical biomass map from Avitabile et al. (2016) with models from the Inter-Sectoral Impact Model Intercomparison Project (ISIMIP) ensemble (Friend et al. 2014; Warszawski et al. 2014). There is a large uncertainty represented by the inter-model spread while they tend to overestimate biomass stocks in regions of the Americas and Africa located north of 10°N and south 15°S. Friend et al. (2014) clearly demonstrated that the highest disagreement between models



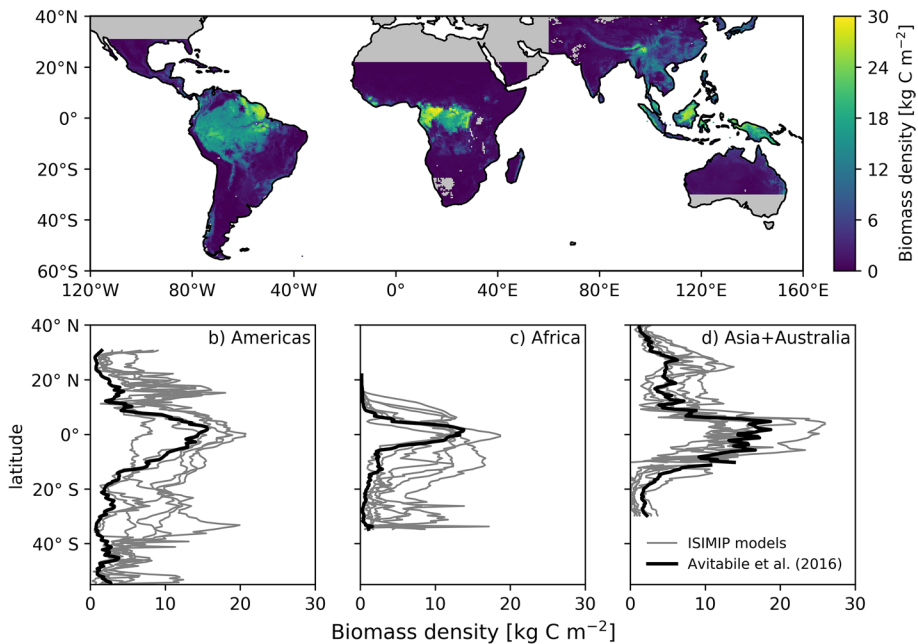


**Fig. 2** Biomass density from Avitabile et al. (2016) (top) and comparison of zonal means simulations (bottom, as indicated) from six Inter-Sectoral Impact Model Intercomparison Project (ISIMIP) ecosystem models. Results indicate an overestimation of stocks by models in the Americas and Africa

resides in the internally modelled residence times of carbon which can be inferred from the ratio between observable fluxes and stocks (Friend et al. 2014; Sierra et al. 2017). Under the same future changes in environmental and climate conditions models alternatively predict longer or shorter turnover times of carbon in vegetation. This mismatch reflects a disagreement in the sign of the terrestrial carbon cycle feedback on future changes in climate and atmospheric  $\text{CO}_2$ . Current EO-based estimates suggest a pervasive control of hydrology on whole ecosystem apparent turnover times of carbon, which are not captured by current Earth system models (Carvalhais et al. 2014). In particular, the spatial patterns of vegetation C turnover times in forests suggest strong climatic controls in mortality patterns associated with drought and heat, but also extreme winter cold temperatures which could expand plant mortality, or reduce it, via reductions in herbivore activity (Thurner et al. 2016). An across-model comparison also revealed that most state-of-the-art global vegetation models do not reflect the direct effects of climate-induced mortality (Thurner et al. 2017), emphasizing the present challenge of understanding mortality induced by climate extreme (Hartmann et al. 2015). Furthermore, recent results have also emphasize the role of land use, in addition to land cover, as a substantial factor for an overall reduction in carbon residence times in terrestrial vegetation (Erb et al. 2016).

In general, all of these works have been emphasizing the mismatch between model and observation-derived ecosystem dynamics and hypothesizing on the missing, or misrepresented, underlying mechanisms that drive carbon dynamics. Downstream, a full body of research has also been focusing on formally integrating these observations into model data assimilation frameworks to maximize information transfer from observation to models.

## 4 Model Data Integration

While EO can be used to benchmark models, they do not measure all aspects of the terrestrial carbon cycle. Therefore, models are needed to fill gaps, but benchmarking studies reviewed in Sect. 3 have generally pointed to poor performances and systematic biases in forward models. Model data integration aims to synergize data and models through an interactive process. There exist multiple forms of model data integration in which EO has been used to provide global covariates for the extrapolation of in situ data (e.g., Jung et al. 2011), retrieve state variables such as LAI from reflectance through a complex radiative transfer scheme (Lewis et al. 2012), constrain productivity and phenology model parameters in terrestrial Carbon Cycle Data Assimilation Systems (CCDAS; e.g., Knorr et al. 2010) or even provide the initial conditions to detailed forest models (e.g., Rödiger et al. 2017, 2018).

The global coverage of EO has allowed the development of a range of “bottom-up” approaches to upscale data-driven in situ models to spatially explicit gridded estimates. One major development in this area has relied on training machine learning algorithm to reproduce local ecosystem fluxes as a function of climate and vegetation properties available from EO (e.g., NDVI, FAPAR). The first example of this approach was reported by Papale and Valentini (2003) who used an Artificial Neural Network trained at 16 European sites to generate continental maps of forest productivity using information about land cover, seasonal temperatures and maximum NDVI from AVHRR. Jung et al. (2009) developed the Model Tree Ensemble (MTE) algorithm to create gridded products of GPP and latent heat fluxes. They first demonstrated the potential for their approach in a synthetic example using LPJmL simulations as training data. Using this method driven by fluxes measured at several FLUXNET sites has allowed the first data-driven description of the distribution of global GPP between biomes and an attribution of dominant regional climate drivers for the period 1998–2005 (Beer et al. 2010). Building on this approach, monthly gridded estimates of GPP extending back to 1982 have been created using GIMMS FAPAR data (Jung et al. 2011). They identified semi-arid and sub-humid as experiencing a high inter-annual variability in productivity due to rainfall variations. These data, used in combination with process-based models, further helped identify the response of savannah ecosystems to ENSO as the dominant driver of the variability in the land carbon sink (Poulter et al. 2014). Multiple machine learning approaches, relying on various algorithms, have been compared by Tramontana et al. (2016). The evaluation of different approaches was performed as part of the FLUXCOM initiative (<http://www.fluxcom.org>). The conclusion of this comparison was that machine learning approaches were skilled at reproducing heat and productivity fluxes but may be biased to predict net ecosystem carbon fluxes due to the lack of feedback representation and knowledge of historical disturbance regimes. Nevertheless, bottom-up and top-down approaches estimates of GPP are in good agreement. Figure 3 presents mean annual GPP estimated by FLUXCOM during 2000–2013 and compares it to the MODIS GPP product. Both approaches are partly driven by the same estimates of MODIS FAPAR which yields a high spatial correlation ( $r=0.80$ ;  $p \ll 0.001$ ). FLUXCOM indicates a mean annual GPP of  $124.7 \text{ Pg C year}^{-1}$  while MODIS estimates a  $136.4 \text{ Pg C year}^{-1}$ , a 9% relative difference.

Beyond empirical approaches, the increasing availability of EO has played a key role in the development of more “top-down” terrestrial Carbon Cycle Data Assimilation Systems (CCDAS). Unlike “bottom-up” approaches which consist in extrapolating in situ models, “top-down” CCDAS are centred around using EO, including non-carbon variables



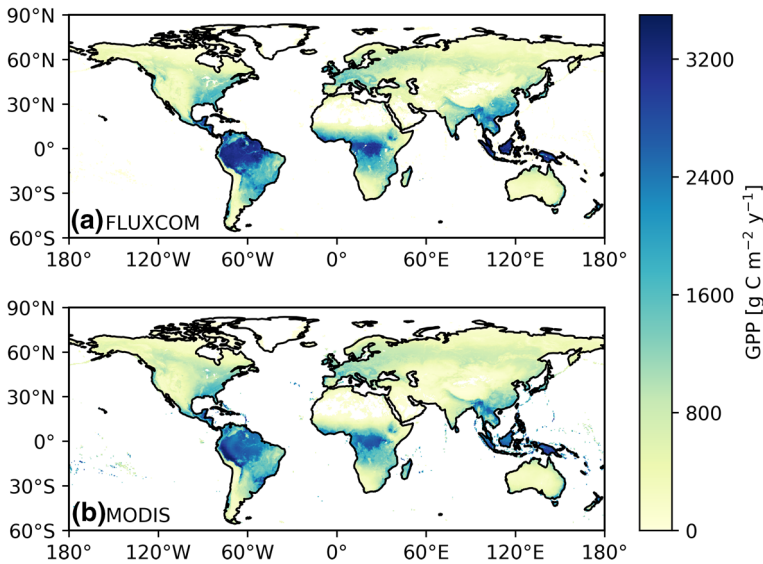


**Fig. 3** Mean annual gross primary production (GPP) during 2000–2013 as reported by **a** the FLUXCOM product and **b** MODIS MOD17 GPP product. FLUXCOM corresponds to eddy covariance data upscaled at  $0.5^\circ$  using machine learning. MODIS product is based on a light use efficiency model and was regridded from  $30''$  ( $\sim 1$  km) to  $0.5^\circ$

(Scholze et al. 2017), to constrain process-based models in a spatially explicit way. One of the first CCDAS was based on the Bethy ecosystem model (Knorr 2000). It has been incrementally improved with additional processes such as dynamic phenology (Knorr et al. 2010). An interesting aspect of CCDAS studies has been to focus on the development and comparison of inversion strategies (e.g., Ziehn et al. 2012) to reduce the computational cost of the assimilation. We refer the reader to a detailed review of the evolution of CCDAS by Kaminski et al. (2013) for more information about this particular framework. One strategy introduced by Peylin et al. (2016) has also been to use a stepwise approach to first constrain parameters related to phenology in the ORCHIDEE model before assimilating fluxes in a subsequent step.

We focus the following paragraphs on examples of new knowledge derived from CCDAS applications and point the readers to the recent review of Scholze et al. (2017) for more technical information about the type of assimilation techniques and EO used. The advantage of EO is that model data integration is performed globally, and CCDAS framework such as CARDAMOM (Bloom et al. 2016) and CASA-GFED (van der Werf et al. 2010) provide compelling methodologies for reconciling land surface and atmospheric constraints on the terrestrial C balance, through which major uncertainties in process representation such as phenology (e.g., Stöckli et al. 2011; Forkel et al. 2014), allocation (Bloom et al. 2016), combustion and emission dynamics (Bloom et al. 2015; Worden et al. 2017a, b) can be explicitly constrained.

Phenology is a poorly represented process, and assimilating reflectance-based EO of NDVI, FAPAR and LAI has allowed in development and validation of new global models. For example, Knorr et al. (2010) assimilated daily FAPAR at seven sites in a generic phenological model. Quaife et al. (2008) demonstrated that assimilating reflectance from the MODIS sensor in the Data Assimilation Linked Ecosystem Carbon model (DALEC;

Williams et al. 2005) led to an improvement in simulated carbon fluxes at a coniferous forest site in Oregon, USA. Stöckli et al. (2011) assimilated 10 years of MODIS LAI and FAPAR data in a phenological model based on the Growing Season Index concept (GSI; Jolly et al. 2005). They identified used the constrained model to produce a 50-year re-analysis of LAI and FAPAR. Forkel et al. (2014) implemented a modified version of the GSI model in the LPJmL dynamic global vegetation model. They retrieved dominant controls of phenology by assimilating 30 years of GIMMS FAPAR, highlighting the codominant role of moisture stress on the variability in phenology (Forkel et al. 2015) which contrasts with classical temperature-based parameterizations. The importance of moisture availability was also found by MacBean et al. (2015) based on the biases in the temperature-driven phenology of the ORCHIDEE model. While these previous studies have relied on plant functional types, Caldararu et al. (2014) successfully fitted a phenological model to pixel-wise MODIS LAI data. Their approach based on carbon optimality concluded that leaf age was also a limiting factor for phenology in evergreen tropical regions.

EO of fire has also been used to constrain emission estimates. Top-down estimates of surface CO emissions amount to a robust constraint on continental-scale fire C emissions: measurements of atmospheric CO—including those from ESA's IASI instrument, NASA's MOPITT, TES and AIRS instruments—have been used to constrain atmospheric chemistry and transport models in data assimilation frameworks (Jiang et al. 2015; Gonzi et al. 2011; Krol et al. 2013; Kopacz et al. 2010, amongst many others). Subsequently, estimates of fire CO:CO<sub>2</sub> ratio (Andreae and Merlet 2001; Akagi et al. 2011) have been used to quantify continental-scale fire C fluxes (Gatti et al. 2014; Bowman et al. 2017). However, CO:CO<sub>2</sub> has been identified as a potential source of error in extreme fire events (Krol et al. 2013; Bloom et al. 2015), where CO:CO<sub>2</sub> values and their uncertainty characteristics are poorly known. Overall, estimates of fire emissions derived from an array of bottom-up and top-down constraints are invaluable for obtaining spatially explicit estimates of fire C fluxes (Bowman et al. 2017; Liu et al. 2017). Ultimately, satellite-based estimation of fire C emissions, characteristics and trends are key to advance process-level understanding of fires as a dynamic component of the Earth system.

Although a number of satellite-derived products (NDVI, LAI, FAPAR, biomass and XCO<sub>2</sub>) have been used to constrain both modelled leaf phenology, biomass and net CO<sub>2</sub> fluxes (Kaminski et al. 2013; Forkel et al. 2015; MacBean et al. 2015; Peylin et al. 2016; Bloom et al. 2016), these data only provide indirect information on gross C uptake. For some vegetation types, even ground-based net CO<sub>2</sub> fluxes derived from eddy covariance towers only provide limited capacity in constraining the gross C fluxes (Kuppel et al. 2014). Consequently, SIF products have been used in a variety of ways to assess and improve land surface model (LSM) simulations: (1) to benchmark GPP and SIF temporal dynamics simulated for a range of sites (Lee et al. 2015; Thum et al. 2017); (2) to optimize global-scale GPP estimates from a LSM inter-comparison a posteriori (Parazoo et al. 2014); and to optimize parameters of both fluorescence and photosynthesis models at local to global scales (Zhang et al. 2014; MacBean et al. 2018; Norton et al. 2018; Norton et al., in review). The latter studies have demonstrated considerable potential for SIF to constrain both in situ and global-scale GPP simulations. MacBean et al. (2018) and Norton et al. (under review) show strong reductions in both the spatio-temporal misfit (increased correlation and decreased bias) across vegetation types between modelled and observed GPP and SIF and the simulated global-scale GPP uncertainty. The reduction in GPP uncertainty is a result of constraining both fluorescence, photosynthesis and phenology-related parameters. In many of the above-mentioned modelling studies, an explicit formulation of the relationship between photosynthesis and fluorescence has been developed—largely based

on the Soil Canopy Observation Photochemistry and Energy Fluxes (SCOPE) model (van der Tol et al. 2009)—and implemented within each respective LSM (Lee et al. 2015; Thum et al. 2017; Norton et al. 2018; Norton et al., in review). However, SIF has been shown to be linearly correlated with GPP at a range of spatial and temporal scales (Frankenberg et al. 2011; Guanter et al. 2012; Joiner et al. 2014; Yang et al. 2015, 2017; Zhang et al. 2016; Wood et al. 2017). This assumed linear relationship also allows a relatively simple and straightforward means by which modelled GPP and SIF can be compared with, and constrained by, remote sensing SIF estimates at large spatial scales (MacBean et al. 2018).

Continental-scale temporal variability of the terrestrial land sink can be robustly observed through atmospheric CO<sub>2</sub> measurements from satellites—most notably from SCIAMACHY instrument onboard ENVISAT, JAXA's GOSAT and the NASA OCO-2 missions (Buchwitz and Burrows 2004; Yokota et al. 2009; Eldering et al. 2017). Terrestrial CO<sub>2</sub> fluxes can be quantitatively retrieved through assimilation of these observations into inverse modelling frameworks (Houweling et al. 2015; Deng et al. 2016), although we note that absolute CO<sub>2</sub> flux estimates are susceptible to a number of model and observation biases (Feng et al. 2016; Miller et al. 2018; Worden et al. 2017b; Basu et al. 2018). Notable insights into terrestrial C cycle processes from satellite-constrained estimates of land C fluxes include multi-year constraints on the Australian C balance (Detmers et al. 2015) regional constraints on the seasonal and inter-annual Amazon C fluxes (Parazoo et al. 2013; Bowman et al. 2017) and Indonesia fire C emissions during the 2015 ENSO (Heymann et al. 2017). Pantropical continental-scale estimates of inter-annual CO<sub>2</sub> flux variations by Liu et al. (2017) demonstrated the synergistic capacity of GOSAT and OCO-2 CO<sub>2</sub> measurements—along with ancillary constraints from solar-induced fluorescence—to disentangle the processes regulating the temporal variability of the terrestrial C sink.

While previous studies have focused on fluxes, reconciling stocks is the key as these are responsible for uncertainty in residence times (Carvalhais et al. 2014; Friend et al. 2014). Bloom et al. (2016) have used pantropical biomass estimates from Saatchi et al. (2011) to constrain global retrievals of carbon allocation and residence times in the CARDAMOM framework. Figure 4 shows an updated version of these data based on the assimilation of biomass estimates from Avitabile et al. (2016) and MODIS LAI for the period 2000–2015. These simulations, limited to the area covered by Avitabile et al. (2016),

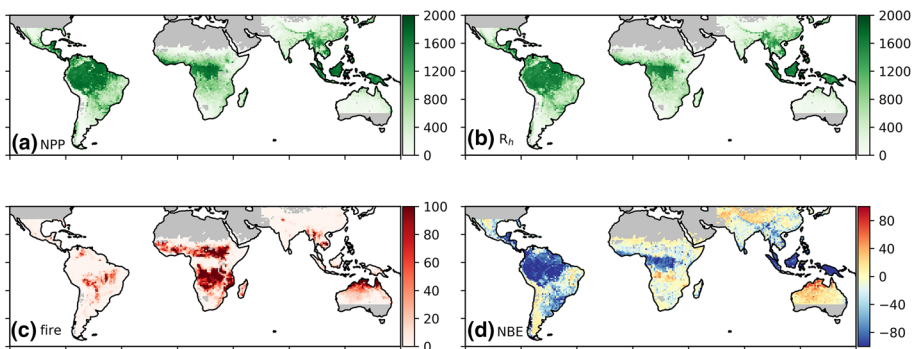


**Fig. 4** CARDAMOM (CARbon DATA MODEL fraMework) retrievals of land–atmosphere C fluxes, averaged over 2000–2015. All fluxes are in g C m<sup>-2</sup>. In d, net biome exchange (NBE) is calculated as  $NBE = -NPP + R_h + \text{fire}$ ; hence, <0 values correspond to a sink (in blue) and >0 correspond to a source of carbon (in red)

provide EO-constrained estimation of NPP ( $43.3 \text{ Pg C year}^{-1}$ ), heterotrophic respiration (Rh;  $40.2 \text{ Pg C year}^{-1}$ ), fire emissions ( $1.2 \text{ Pg C year}^{-1}$ ) and Net Biome Exchange ( $-1.7 \text{ Pg C year}^{-1}$ , corresponding to a sink) as reported in Exbrayat et al. (2018b).

Furthermore, an accurate representation of stocks in ecosystem models is required to robustly estimate emissions related to land use change. Li et al. (2017) used estimates of current biomass compiled by Carvalhais et al. (2014) to constrain centennial emissions from land use change in an ensemble of nine models. While global numbers of cumulative emissions from land use change were similar between the unconstrained and constrained models, regional differences appeared. For example, the data-constrained estimates yielded larger emissions from land use change in the tropics and smaller in temperate regions, compared to the unconstrained estimates. In a more recent study, Lienert and Joos (2018) also used biomass data from Carvalhais et al. (2014) to constrain emissions from land use change using alternative representation of emissions due to net and/or gross land use transitions.

Studies presented in previous paragraphs have focused on using EO data to constrain fluxes and state variables in conceptual models. However, remotely sensed information of vegetation structure can be connected to highly detailed forest models to provide mechanistic estimates of forest biomass and productivity (Shugart et al. 2015; Knapp et al. 2018a, b). Forest structure is indeed an important element to describe the state of forests. Precise estimates of forest structure need to consider small-scale variations resulting from local disturbances, on the one hand, and require large-scale information on the state of the forest that can be detected by remote sensing, on the other hand (Rödig et al. 2017). Local forest models can simulate and analyse different kinds of local disturbances and thus small-scale changes in forest structures more accurately than global ecosystem models. Remote sensing has the potential to provide global high-resolution measurements of the structure of a forest (e.g., forest height by LIDAR or interferometric radar measurements).

As an example, Rödig et al. (2017) used remote sensing data with a resolution of  $1 \text{ km}^2$  (i.e. canopy height map derived from ICESat) to establish large-scale applications of a local forest gap model (i.e. FORMIND, Fischer et al. 2016). Forest gap models (Shugart et al. 2018) simulate forest succession at the individual tree level. The advantage of using a local forest model at the large scale is that it brings along information on many different forest attributes (e.g., productivity, carbon sequestration, water fluxes) in a very fine resolution. In combination with remote sensing, this enables the derivation of high-resolution maps of carbon stocks and fluxes—which was conducted for the whole Amazon (Rödig et al. 2017, 2018). By this approach, it was possible to simulate each tree in the Amazon. Finally growth of more than 410 billion trees was analysed. According to this study, forests in the Amazon store high amounts of above-ground biomass (76 Gt of carbon) and are an important sink of  $0.56 \text{ Gt C a}^{-1}$  under current conditions (Rödig et al. 2018).

## 5 Outlook

EO has made an essential contribution to our understanding of the terrestrial carbon cycle since the 1980s. It ranges from the continuous monitoring of vegetation activity through NDVI, FAPAR and LAI to providing wall-to-wall constraints for model-based estimates of land–atmosphere carbon fluxes. Nowadays, multiple dedicated missions and services, such as the Sentinel satellites of the European Union's Copernicus programme, provide almost real-time observations with a high level of quality. For example, the ESA TROPOMI

instrument of Sentinel-5P provides CO measurements with an unprecedented spatio-temporal coverage (Borsdorff et al. 2018). In the next few years, multiple sensors will be launched to complement the existing constellation of Sentinels and provide coincident observations of several aspects of the biosphere (Stavros et al. 2017).

NASA's Global Ecosystem Dynamics Investigation (GEDI) mission, a LIDAR system on board the International Space Station (ISS), will provide a global coverage of canopy height and foliage vertical profiles. It will provide updated and more detailed structural information for integration with forest models (e.g., Rödiger et al. 2017, 2018). ESA's 7th Earth Explorer BIOMASS (Le Toan et al. 2011) will provide repeated measurements of tropical biomass with a P-band synthetic aperture radar. In contrast to currently available biomass maps, temporally resolved information losses from deforestation and gain from regrowth will be especially useful to reduce the uncertainty and correct bias in CCDAS framework (Smallman et al. 2017).

Recent studies have demonstrated the potential for satellite CO<sub>2</sub> observations to constrain land–atmosphere exchange (Liu et al. 2017). NASA's upcoming OCO-3 will replace OCO-2 on board the ISS, while the geostationary GeoCARB will focus on the Americas. Both systems, and the dedicated ESA's Fluorescence Explorer (FLEX) mission, will provide measurements of SIF which has a great potential to constrain models of ecosystem productivity (MacBean et al. 2018), especially following the implementation of mechanistic representation of leaf physiology in CCDAS (Norton et al. 2018).

Finally, the carbon cycle is tightly linked to the energy and water cycles semi-arid areas in particular have been pointed as key ecosystems to understand the global land carbon sink (Poulter et al. 2014). Therefore, the development of new non-carbon EO and their assimilation in CCDAS frameworks plays a major role in simulating the carbon cycle (Scholze et al. 2017). NASA's ECOSTRESS will measure evapotranspiration (Stavros et al. 2017) which will be used to obtain estimates of water-use efficiency, the ratio of productivity to evapotranspiration, which will be useful to drive process-based models of the biosphere.

Overall, the next few years will see an increase in the amount of observing systems with a ever-increasing spatial resolution and higher frequency. One of the key challenges for the modelling community is to build systems able to ingest all this information in an efficient way to provide high confidence retrievals of the terrestrial carbon cycle.

**Acknowledgements** This review stemmed from the workshop “Space-based Measurement of Forest Properties for Carbon Cycle Research” at the International Space Science Institute in Bern during November 2017. Contribution from AAB was carried out at the Jet Propulsion Laboratory, California Institute of Technology, under a contract with the National Aeronautics and Space Administration. The first and last authors were supported by the Natural Environment Research Council through the National Centre for Earth Observation, contract number PR140015, and the Newton Fund, through CSSP Brazil.

## References

- Akagi SK, Yokelson RJ, Wiedinmyer C et al (2011) Emission factors for open and domestic biomass burning for use in atmospheric models. *Atmos Chem Phys* 11:4039–4072. <https://doi.org/10.5194/acp-11-4039-2011>
- Anav A, Friedlingstein P, Kidston M et al (2013) Evaluating the land and ocean components of the global carbon cycle in the CMIP5 earth system models. *J Clim* 26:6801–6843. <https://doi.org/10.1175/JCLI-D-12-00417.1>
- Andela N, Morton DC, Giglio L et al (2017) A human-driven decline in global burned area. *Science* 356:1356–1362. <https://doi.org/10.1126/science.aal4108>

- Andreae MO, Merlet P (2001) Emission of trace gases and aerosols from biomass burning. *Glob Biogeochem Cycles* 15:955–966. <https://doi.org/10.1029/2000GB001382>
- Archibald S, Lehmann CER, Gómez-Dans JL, Bradstock RA (2013) Defining pyromes and global syndromes of fire regimes. *Proc Natl Acad Sci USA* 110:6442–7. <https://doi.org/10.1073/pnas.1211466110>
- Arneith A, Sitch S, Pongratz J et al (2017) Historical carbon dioxide emissions caused by land-use changes are possibly larger than assumed. *Nat Geosci* 10:79–84. <https://doi.org/10.1038/ngeo2882>
- Arora VK, Melton JR (2018) Reduction in global area burned and wildfire emissions since 1930s enhances carbon uptake by land. *Nat Commun* 9:1326. <https://doi.org/10.1038/s41467-018-03838-0>
- Arora VK, Boer GJ, Friedlingstein P et al (2013) Carbon-concentration and carbon-climate feedbacks in CMIP5 earth system models. *J Clim* 26:5289–5314. <https://doi.org/10.1175/JCLI-D-12-00494.1>
- Avitabile V, Herold M, Heuvelink GBM et al (2016) An integrated pan-tropical biomass map using multiple reference datasets. *Glob Change Biol* 22:1406–1420. <https://doi.org/10.1111/gcb.13139>
- Baccini A, Goetz SJ, Walker WS et al (2012) Estimated carbon dioxide emissions from tropical deforestation improved by carbon-density maps. *Nat Clim Change* 2:182–185. <https://doi.org/10.1038/nclimate1354>
- Baccini A, Walker W, Carvalho L et al (2017) Tropical forests are a net carbon source based on aboveground measurements of gain and loss. *Science* (80) 358:230–234. <https://doi.org/10.1126/science.aam5962>
- Baldocchi D, Falge E, Gu LH et al (2001) FLUXNET: a new tool to study the temporal and spatial variability of ecosystem-scale carbon dioxide, water vapor, and energy flux densities. *Bull Am Meteorol Soc* 82:2415–2434. [https://doi.org/10.1175/1520-0477\(2001\)082%3c2415:FANTTS%3e2.3.CO;2](https://doi.org/10.1175/1520-0477(2001)082%3c2415:FANTTS%3e2.3.CO;2)
- Baret F, Weiss M, Lacaze R et al (2013) GEOV1: LAI and FAPAR essential climate variables and FCOVER global time series capitalizing over existing products. Part 1: principles of development and production. *Remote Sens Environ* 137:299–309. <https://doi.org/10.1016/J.RSE.2012.12.027>
- Bastos A, Running SW, Gouveia C, Trigo RM (2013) The global NPP dependence on ENSO: La Niña and the extraordinary year of 2011. *J Geophys Res Biogeosci* 118:1247–1255. <https://doi.org/10.1002/jgrg.20100>
- Bastos A, Gouveia CM, Trigo RM, Running SW (2014) Analysing the spatio-temporal impacts of the 2003 and 2010 extreme heatwaves on plant productivity in Europe. *Biogeosciences* 11:3421–3435. <https://doi.org/10.5194/bg-11-3421-2014>
- Bastos A, Ciais P, Park T et al (2017) Was the extreme Northern Hemisphere greening in 2015 predictable? *Environ Res Lett* 12:44016. <https://doi.org/10.1088/1748-9326/aa67b5>
- Basu S, Baker DF, Chevallier F et al (2018) The impact of transport model differences on CO<sub>2</sub> surface flux estimates from OCO-2 retrievals of column average CO<sub>2</sub>. *Atmos Chem Phys* 18:7189–7215. <https://doi.org/10.5194/acp-18-7189-2018>
- Beer C, Reichstein M, Tomelleri E et al (2010) Terrestrial gross carbon dioxide uptake: global distribution and covariation with climate. *Science* 329:834–838. <https://doi.org/10.1126/science.1184984>
- Bloom AA, Worden J, Jiang Z et al (2015) Remote-sensing constraints on South America fire traits by Bayesian fusion of atmospheric and surface data. *Geophys Res Lett* 42:1268–1274. <https://doi.org/10.1002/2014GL062584>
- Bloom AA, Exbrayat J-F, van der Velde IR, Feng L, Williams M (2016) The decadal state of the terrestrial carbon cycle: global retrievals of terrestrial carbon allocation, pools, and residence times. *Proc Natl Acad Sci* 113(5):1285–1290. <https://doi.org/10.1073/pnas.1515160113>
- Borsdorff T, Aan de Brugh J, Hu H et al (2018) Measuring carbon monoxide with TROPOMI: first results and a comparison with ECMWF-IFS analysis data. *Geophys Res Lett* 45:2826–2832. <https://doi.org/10.1002/2018GL077045>
- Bowman KW, Liu J, Bloom AA et al (2017) Global and Brazilian carbon response to El Niño Modoki 2011–2010. *Earth Space Sci* 4:637–660. <https://doi.org/10.1002/2016EA000204>
- Brandt M, Wigneron J-P, Chave J et al (2018) Satellite passive microwaves reveal recent climate-induced carbon losses in African drylands. *Nat Ecol Evol* 2:827–835. <https://doi.org/10.1038/s41559-018-0530-6>
- Broich M, Huete A, Tulbure MG et al (2014) Land surface phenological response to decadal climate variability across Australia using satellite remote sensing. *Biogeosciences* 11:5181–5198. <https://doi.org/10.5194/bg-11-5181-2014>
- Buchwitz M, Burrows JP (2004) Retrieval of CH<sub>4</sub>, CO, and CO<sub>2</sub> total column amounts from SCIAMACHY near-infrared nadir spectra: retrieval algorithm and first results. In: Schaefer K, Comeron A, Carleer MR, Picard RH (eds) *Proceedings of SPIE*, p 375
- Buitenwerf R, Rose L, Higgins SI (2015) Three decades of multi-dimensional change in global leaf phenology. *Nat Clim Change* 5:364–368. <https://doi.org/10.1038/nclimate2533>



- Caldararu S, Purves DW, Palmer PI (2014) Phenology as a strategy for carbon optimality: a global model. *Biogeosciences* 11:763–778. <https://doi.org/10.5194/bg-11-763-2014>
- Canadell JG, Le Quéré C, Raupach MR et al (2007) Contributions to accelerating atmospheric CO<sub>2</sub> growth from economic activity, carbon intensity, and efficiency of natural sinks. *Proc Natl Acad Sci USA* 104:18866–18870. <https://doi.org/10.1073/pnas.0702737104>
- Carvalhais N, Forkel M, Khomik M et al (2014) Global covariation of carbon turnover times with climate in terrestrial ecosystems. *Nature* 514:213–217. <https://doi.org/10.1038/nature13731>
- Chave J, Coomes D, Jansen S et al (2009) Towards a worldwide wood economics spectrum. *Ecol Lett* 12:351–366. <https://doi.org/10.1111/j.1461-0248.2009.01285.x>
- Chave J, Réjou-Méchain M, Búrquez A et al (2014) Improved allometric models to estimate the above-ground biomass of tropical trees. *Glob Change Biol* 20:3177–3190. <https://doi.org/10.1111/gcb.12629>
- Clark DB, Mercado LM, Sitch S et al (2011) The joint UK land environment simulator (JULES), model description—part 2: carbon fluxes and vegetation dynamics. *Geosci Model Dev* 4:701–722. <https://doi.org/10.5194/gmd-4-701-2011>
- Dannenberg MP, Wise EK, Janko M et al (2018) Atmospheric teleconnection influence on North American land surface phenology. *Environ Res Lett* 13:34029. <https://doi.org/10.1088/1748-9326/aaa85a>
- Deng F, Jones DBA, O'Dell CW et al (2016) Combining GOSAT×CO<sub>2</sub> observations over land and ocean to improve regional CO<sub>2</sub> flux estimates. *J Geophys Res Atmos* 121:1896–1913. <https://doi.org/10.1002/2015JD024157>
- Detmers RG, Hasekamp O, Aben I et al (2015) Anomalous carbon uptake in Australia as seen by GOSAT. *Geophys Res Lett* 42:8177–8184. <https://doi.org/10.1002/2015GL065161>
- Eldering A, Wennberg PO, Crisp D et al (2017) The orbiting carbon observatory-2 early science investigations of regional carbon dioxide fluxes. *Science* 358:eaam5745. <https://doi.org/10.1126/science.aam5745>
- Erb K-H, Fetzel T, Plutzar C et al (2016) Biomass turnover time in terrestrial ecosystems halved by land use. *Nat Geosci* 9:674–678. <https://doi.org/10.1038/ngeo2782>
- Exbrayat J-F, Williams M (2015) Quantifying the net contribution of the historical Amazonian deforestation to climate change. *Geophys Res Lett* 42:2968–2976. <https://doi.org/10.1002/2015GL063497>
- Exbrayat J-F, Pitman AJ, Abramowitz G (2014) Response of microbial decomposition to spin-up explains CMIP5 soil carbon range until 2100. *Geosci Model Dev* 7:2683–2692. <https://doi.org/10.5194/gmd-7-2683-2014>
- Exbrayat J-F, Liu YY, Williams M (2017) Impact of deforestation and climate on the Amazon Basin's above-ground biomass during 1993–2012. *Sci Rep* 7:15615. <https://doi.org/10.1038/s41598-017-15788-6>
- Exbrayat J-F, Anthony Bloom A, Falloon P et al (2018a) Reliability ensemble averaging of 21st century projections of terrestrial net primary productivity reduces global and regional uncertainties. *Earth Syst Dyn* 9:1. <https://doi.org/10.5194/esd-9-153-2018>
- Exbrayat J-F, Smallman TL, Anthony Bloom A, Hutley LB, Williams M (2018b) Inverse determination of the influence of fire on vegetation carbon turnover in the pantropics. *Glob Biogeochem Cycles* 32(12):1776–1789. <https://doi.org/10.1029/2018GB005925>
- Fasullo JT, Boening C, Landerer FW, Nerem RS (2013) Australia's unique influence on global sea level in 2010–2011. *Geophys Res Lett* 40:4368–4373. <https://doi.org/10.1002/grl.50834>
- Feng L, Palmer PI, Parker RJ et al (2016) Estimates of European uptake of CO<sub>2</sub> inferred from GOSAT×CO<sub>2</sub> retrievals: sensitivity to measurement bias inside and outside Europe. *Atmos Chem Phys* 16:1289–1302. <https://doi.org/10.5194/acp-16-1289-2016>
- Field CB, Randerson JT, Malmström CM (1995) Global net primary production: combining ecology and remote sensing. *Remote Sens Environ* 51:74–88. [https://doi.org/10.1016/0034-4257\(94\)00066-V](https://doi.org/10.1016/0034-4257(94)00066-V)
- Fischer R, Bohn F, Dantas de Paula M et al (2016) Lessons learned from applying a forest gap model to understand ecosystem and carbon dynamics of complex tropical forests. *Ecol Modell* 326:124–133. <https://doi.org/10.1016/j.ecolmodel.2015.11.018>
- Flannigan MD, Haar THV (1986) Forest fire monitoring using NOAA satellite AVHRR. *Can J For Res* 16:975–982. <https://doi.org/10.1139/x86-171>
- Forkel M, Carvalhais N, Schaphoff S et al (2014) Identifying environmental controls on vegetation greenness phenology through model-data integration. *Biogeosciences* 11:7025–7050. <https://doi.org/10.5194/bg-11-7025-2014>
- Forkel M, Migliavacca M, Thonicke K et al (2015) Codominant water control on global interannual variability and trends in land surface phenology and greenness. *Glob Change Biol* 21:3414–3435. <https://doi.org/10.1111/gcb.12950>

- Forkel M, Carvalhais N, Rodenbeck C et al (2016) Enhanced seasonal CO<sub>2</sub> exchange caused by amplified plant productivity in northern ecosystems. *Science* 351:696–699. <https://doi.org/10.1126/science.aac4971>
- Frankenberg C, Fisher JB, Worden J et al (2011) New global observations of the terrestrial carbon cycle from GOSAT: patterns of plant fluorescence with gross primary productivity. *Geophys Res Lett* 1:1. <https://doi.org/10.1029/2011gl048738>
- Freeborn PH, Wooster MJ, Roy DP, Cochrane MA (2014) Quantification of MODIS fire radiative power (FRP) measurement uncertainty for use in satellite-based active fire characterization and biomass burning estimation. *Geophys Res Lett* 41:1988–1994. <https://doi.org/10.1002/2013GL059086>
- Friedlingstein P, Cox P, Betts R et al (2006) Climate-carbon cycle feedback analysis: results from the C4MIP model intercomparison. *J Clim* 19:3337–3353. <https://doi.org/10.1175/JCLI3800.1>
- Friend AD, Lucht W, Rademacher TT et al (2014) Carbon residence time dominates uncertainty in terrestrial vegetation responses to future climate and atmospheric CO<sub>2</sub>. *Proc Natl Acad Sci USA* 111:3280–3285. <https://doi.org/10.1073/pnas.1222477110>
- Gatti LV, Gloor M, Miller JB et al (2014) Drought sensitivity of Amazonian carbon balance revealed by atmospheric measurements. *Nature* 506:76–80. <https://doi.org/10.1038/nature12957>
- Giglio L, Randerson JT, van der Werf GR (2013) Analysis of daily, monthly, and annual burned area using the fourth-generation global fire emissions database (GFED4). *J Geophys Res Biogeosci* 118:317–328. <https://doi.org/10.1002/jgrg.20042>
- Giorgi F, Mearns LO (2002) Calculation of average, uncertainty range, and reliability of regional climate changes from AOGCM simulations via the “reliability ensemble averaging” (REA) method. *J Clim* 15:1141–1158. [https://doi.org/10.1175/1520-0442\(2002\)015%3c1141:COAURA%3e2.0.CO;2](https://doi.org/10.1175/1520-0442(2002)015%3c1141:COAURA%3e2.0.CO;2)
- Gonzi S, Feng L, Palmer PI (2011) Seasonal cycle of emissions of CO inferred from MOPITT profiles of CO: sensitivity to pyroconvection and profile retrieval assumptions. *Geophys Res Lett* 38:1–11. <https://doi.org/10.1029/2011gl046789>
- Guanter L, Frankenberg C, Dudhia A et al (2012) Retrieval and global assessment of terrestrial chlorophyll fluorescence from GOSAT space measurements. *Remote Sens Environ* 121:236–251. <https://doi.org/10.1016/j.rse.2012.02.006>
- Haarsma RJ, Roberts MJ, Vidale PL et al (2016) High resolution model intercomparison project (HighResMIP v1.0) for CMIP6. *Geosci Model Dev* 9:4185–4208. <https://doi.org/10.5194/gmd-9-4185-2016>
- Hansen MC, Potapov PV, Moore R et al (2013) High-resolution global maps of 21st-century forest cover change. *Science* 342:850–853. <https://doi.org/10.1126/science.1244693>
- Harris NL, Brown S, Hagen SC et al (2012) Baseline map of carbon emissions from deforestation in tropical regions. *Science* 336:1573–1576. <https://doi.org/10.1126/science.1217962>
- Hartmann H, Adams HD, Anderegg WRL et al (2015) Research frontiers in drought-induced tree mortality: crossing scales and disciplines. *New Phytol* 205:965–969. <https://doi.org/10.1111/nph.13246>
- Heymann J, Reuter M, Buchwitz M et al (2017) CO<sub>2</sub> emission of Indonesian fires in 2015 estimated from satellite-derived atmospheric CO<sub>2</sub> concentrations. *Geophys Res Lett* 45:1621. <https://doi.org/10.1002/2016gl072042>
- Houweling S, Baker D, Basu S et al (2015) An intercomparison of inverse models for estimating sources and sinks of CO<sub>2</sub> using GOSAT measurements. *J Geophys Res Atmos* 120:5253–5266. <https://doi.org/10.1002/2014JD022962>
- Huete A, Didan K, Miura T et al (2002) Overview of the radiometric and biophysical performance of the MODIS vegetation indices. *Remote Sens Environ* 83:195–213. [https://doi.org/10.1016/S0034-4257\(02\)00096-2](https://doi.org/10.1016/S0034-4257(02)00096-2)
- Huete AR, Didan K, Shimabukuro YE et al (2006) Amazon rainforests green-up with sunlight in dry season. *Geophys Res Lett* 33:L06405. <https://doi.org/10.1029/2005GL025583>
- Huntzinger DN, Schwalm C, Michalak AM et al (2013) The North American carbon program multi-scale synthesis and terrestrial model intercomparison project ? Part 1: overview and experimental design. *Geosci Model Dev* 6:2121–2133. <https://doi.org/10.5194/gmd-6-2121-2013>
- Ito A, Nishina K, Reyer CPO et al (2017) Photosynthetic productivity and its efficiencies in ISIMIP2a biome models: benchmarking for impact assessment studies. *Environ Res Lett* 12:085001. <https://doi.org/10.1088/1748-9326/aa7a19>
- Jiang Z, Jones DBA, Worden HM, Henze DK (2015) Sensitivity of top-down CO source estimates to the modeled vertical structure in atmospheric CO. *Atmos Chem Phys* 15:1521–1537. <https://doi.org/10.5194/acp-15-1521-2015>
- Joiner J, Guanter L, Lindström R et al (2013) Global monitoring of terrestrial chlorophyll fluorescence from moderate-spectral-resolution near-infrared satellite measurements: methodology, simulations, and application to GOME-2. *Atmos Meas Tech* 6:2803–2823. <https://doi.org/10.5194/amt-6-2803-2013>

- Joiner J, Yoshida Y, Vasilkov AP et al (2014) The seasonal cycle of satellite chlorophyll fluorescence observations and its relationship to vegetation phenology and ecosystem atmosphere carbon exchange. *Remote Sens Environ* 152:375–391. <https://doi.org/10.1016/j.rse.2014.06.022>
- Joiner J, Yoshida Y, Guanter L, Middleton EM (2016) New methods for the retrieval of chlorophyll red fluorescence from hyperspectral satellite instruments: simulations and application to GOME-2 and SCIAMACHY. *Atmos Meas Tech* 9:3939–3967. <https://doi.org/10.5194/amt-9-3939-2016>
- Jolly WM, Nemani R, Running SW (2005) A generalized, bioclimatic index to predict foliar phenology in response to climate. *Glob Change Biol* 11:619–632. <https://doi.org/10.1111/j.1365-2486.2005.00930.x>
- Jung M, Reichstein M, Bondeau A (2009) Towards global empirical upscaling of FLUXNET eddy covariance observations: validation of a model tree ensemble approach using a biosphere model. *Biogeosciences* 6:2001–2013. <https://doi.org/10.5194/bg-6-2001-2009>
- Jung M, Reichstein M, Margolis HA et al (2011) Global patterns of land-atmosphere fluxes of carbon dioxide, latent heat, and sensible heat derived from eddy covariance, satellite, and meteorological observations. *J Geophys Res* 116:G00J07. <https://doi.org/10.1029/2010jg001566>
- Kala J, Decker M, Exbrayat J-F et al (2014) Influence of leaf area index prescriptions on simulations of heat, moisture, and carbon fluxes. *J Hydrometeorol* 15:489–503. <https://doi.org/10.1175/JHM-D-13-063.1>
- Kaminski T, Knorr W, Schürmann G et al (2013) The BETHY/JSBACH carbon cycle data assimilation system: experiences and challenges. *J Geophys Res Biogeosci* 118:1414. <https://doi.org/10.1002/jgrg.20118>
- Knapp N, Fischer R, Huth A (2018a) Linking lidar and forest modeling to assess biomass estimation across scales and disturbance states. *Remote Sens Environ* 205:199–209. <https://doi.org/10.1016/j.rse.2017.11.018>
- Knapp N, Huth A, Kugler F et al (2018b) Model-assisted estimation of tropical forest biomass change: a comparison of approaches. *Remote Sens* 10:731. <https://doi.org/10.3390/rs10050731>
- Knorr W (2000) Annual and interannual CO<sub>2</sub> exchanges of the terrestrial biosphere: process-based simulations and uncertainties. *Glob Ecol Biogeogr* 9:225–252. <https://doi.org/10.1046/j.1365-2699.2000.00159.x>
- Knorr W, Kaminski T, Scholze M et al (2010) Carbon cycle data assimilation with a generic phenology model. *J Geophys Res* 115:G04017. <https://doi.org/10.1029/2009JG001119>
- Knyazikhin Y, Martonchik JV, Myneni RB et al (1998) Synergistic algorithm for estimating vegetation canopy leaf area index and fraction of absorbed photosynthetically active radiation from MODIS and MISR data. *J Geophys Res Atmos* 103:32257–32275. <https://doi.org/10.1029/98JD02462>
- Köhler P, Joiner J (2015) A linear method for the retrieval of sun-induced chlorophyll fluorescence from GOME-2 and SCIAMACHY data. *Atmos Meas Tech* 8:2589–2608. <https://doi.org/10.5194/amt-8-2589-2015>
- Kolby Smith W, Reed SC, Cleveland CC et al (2016) Large divergence of satellite and earth system model estimates of global terrestrial CO<sub>2</sub> fertilization. *Nat Clim Change* 6:306–310. <https://doi.org/10.1038/nclimate2879>
- Kopacz M, Jacob DJ, Fisher JA et al (2010) Global estimates of CO sources with high resolution by adjoint inversion of multiple satellite datasets (MOPITT, AIRS, SCIAMACHY, TES). *Atmos Chem Phys* 10:855–876. <https://doi.org/10.5194/acp-10-855-2010>
- Krishnamurti TN, Kishtawal CM, LaRow TE et al (1999) Improved weather and seasonal climate forecasts from multimodel superensemble. *Science* 285:1548–1550. <https://doi.org/10.1126/science.285.5433.1548>
- Krol M, Peters W, Hooghiemstra P et al (2013) How much CO was emitted by the 2010 fires around Moscow? *Atmos Chem Phys* 13:4737–4747. <https://doi.org/10.5194/acp-13-4737-2013>
- Kuppel S, Peylin P, Maignan F et al (2014) Model-data fusion across ecosystems: from multisite optimizations to global simulations. *Geosci Model Dev* 7:2581–2597. <https://doi.org/10.5194/gmd-7-2581-2014>
- Le Quéré C, Andrew RM, Friedlingstein P et al (2018) Global carbon budget 2017. *Earth Syst Sci Data* 10:405–448. <https://doi.org/10.5194/essd-10-405-2018>
- Le Toan T, Quegan S, Davidson MWJWJ et al (2011) The BIOMASS mission: mapping global forest biomass to better understand the terrestrial carbon cycle. *Remote Sens Environ* 115:2850–2860. <https://doi.org/10.1016/j.rse.2011.03.020>
- Lee J-E, Berry JA, van der Tol C et al (2015) Simulations of chlorophyll fluorescence incorporated into the community land model version 4. *Glob Change Biol* 21:3469–3477. <https://doi.org/10.1111/gcb.12948>
- Lewis P, Gómez-Dans J, Kaminski T et al (2012) An earth observation land data assimilation system (EOLDS). *Remote Sens Environ* 120:219–235. <https://doi.org/10.1016/j.rse.2011.12.027>

- Li W, Ciais P, Peng S et al (2017) Land-use and land-cover change carbon emissions between 1901 and 2012 constrained by biomass observations. *Biogeosciences* 14:5053–5067. <https://doi.org/10.5194/bg-14-5053-2017>
- Lienert S, Joos F (2018) A Bayesian ensemble data assimilation to constrain model parameters and land-use carbon emissions. *Biogeosciences* 15:2909–2930. <https://doi.org/10.5194/bg-15-2909-2018>
- Liu YY, van Dijk AIJM, de Jeu RAM et al (2015) Recent reversal in loss of global terrestrial biomass. *Nat Clim Change* 5:470–474. <https://doi.org/10.1038/nclimate2581>
- Liu J, Bowman KW, Schimel DS et al (2017) Contrasting carbon cycle responses of the tropical continents to the 2015–2016 El Niño. *Science* eaam358:5690. <https://doi.org/10.1126/science.aam5690>
- MacBean N, Maignan F, Peylin P et al (2015) Using satellite data to improve the leaf phenology of a global terrestrial biosphere model. *Biogeosciences* 12:7185–7208. <https://doi.org/10.5194/bg-12-7185-2015>
- MacBean N, Maignan F, Bacour C et al (2018) Strong constraint on modelled global carbon uptake using solar-induced chlorophyll fluorescence data. *Sci Rep*. <https://doi.org/10.1038/s41598-018-20024-w>
- Migliavacca M, Sonnentag O, Keenan TF et al (2012) On the uncertainty of phenological responses to climate change, and implications for a terrestrial biosphere model. *Biogeosciences* 9:2063–2083. <https://doi.org/10.5194/bg-9-2063-2012>
- Miller SM, Michalak AM, Yadav V, Tadić JM (2018) Characterizing biospheric carbon balance using CO<sub>2</sub> observations from the OCO-2 satellite. *Atmos Chem Phys* 18:6785–6799. <https://doi.org/10.5194/acp-18-6785-2018>
- Morton DC, Le Page Y, DeFries R et al (2013) Understorey fire frequency and the fate of burned forests in southern Amazonia. *Philos Trans R Soc B Biol Sci* 368:20120163. <https://doi.org/10.1098/rstb.2012.0163>
- Myneni RB, Hall FG, Sellers PJ, Marshak AL (1995) The interpretation of spectral vegetation indexes. *IEEE Trans Geosci Remote Sens* 33:481–486. <https://doi.org/10.1109/36.377948>
- Myneni RB, Keeling CD, Tucker CJ et al (1997) Increased plant growth in the northern high latitudes from 1981 to 1991. *Nature* 386:698–702. <https://doi.org/10.1038/386698a0>
- Myneni RB, Hoffman S, Knyazikhin Y et al (2002) Global products of vegetation leaf area and fraction absorbed PAR from year one of MODIS data. *Remote Sens Environ* 83:214–231. [https://doi.org/10.1016/S0034-4257\(02\)00074-3](https://doi.org/10.1016/S0034-4257(02)00074-3)
- Myneni RB, Yang W, Nemani RR et al (2007) Large seasonal swings in leaf area of Amazon rainforests. *Proc Natl Acad Sci* 104:4820–4823. <https://doi.org/10.1073/pnas.0611338104>
- New M, Lister D, Hulme M, Makin I (2002) A high-resolution data set of surface climate over global land areas. *Clim Res* 21:1–25. <https://doi.org/10.3354/cr021001>
- Norton AJ, Rayner PJ, Koffi EN, Scholze M (2018a) Assimilating solar-induced chlorophyll fluorescence into the terrestrial biosphere model BETHY-SCOPE v1.0: model description and information content. *Geosci Model Dev* 11:1517–1536. <https://doi.org/10.5194/gmd-11-1517-2018>
- Norton AJ, Rayner PJ, Koffi EN et al (2018b) Estimating global gross primary productivity using chlorophyll fluorescence and a data assimilation system with the BETHY-SCOPE model. *Biogeosciences* 12:835. <https://doi.org/10.5194/bg-2018-270>
- Papale D, Valentini R (2003) A new assessment of European forests carbon exchanges by eddy fluxes and artificial neural network spatialization. *Glob Change Biol* 9:525–535. <https://doi.org/10.1046/j.1365-2486.2003.00609.x>
- Parazoo NC, Bowman K, Frankenberg C et al (2013) Interpreting seasonal changes in the carbon balance of southern Amazonia using measurements of XCO<sub>2</sub> and chlorophyll fluorescence from GOSAT. *Geophys Res Lett* 40:2829–2833. <https://doi.org/10.1002/grl.50452>
- Parazoo NC, Bowman K, Fisher JB et al (2014) Terrestrial gross primary production inferred from satellite fluorescence and vegetation models. *Glob Change Biol* 20:3103–3121. <https://doi.org/10.1111/gcb.12652>
- Peylin P, Bacour C, MacBean N et al (2016) A new stepwise carbon cycle data assimilation system using multiple data streams to constrain the simulated land surface carbon cycle. *Geosci Model Dev* 9:3321–3346. <https://doi.org/10.5194/gmd-9-3321-2016>
- Pinzon JE, Tucker CJ (2014) A non-stationary 1981–2012 AVHRR NDVI3g time series. *Remote Sens* 6:6929–6960. <https://doi.org/10.3390/rs6086929>
- Pitman AJ (2003) The evolution of, and revolution in, land surface schemes designed for climate models. *Int J Climatol* 23:479–510. <https://doi.org/10.1002/joc.893>
- Porcar-Castell A, Tyystjärvi E, Atherton J et al (2014) Linking chlorophyll a fluorescence to photosynthesis for remote sensing applications: mechanisms and challenges. *J Exp Bot* 65:4065–4095. <https://doi.org/10.1093/jxb/eru191>
- Potapov P, Yaroshenko A, Turubanova S et al (2008) Mapping the world's intact forest landscapes by remote sensing. *Ecol Soc* 13:51. <https://doi.org/10.5751/es-02670-130251>

- Potter CS, Randerson JT, Field CB et al (1993) Terrestrial ecosystem production: a process model based on global satellite and surface data. *Glob Biogeochem Cycles* 7:811–841. <https://doi.org/10.1029/93GB02725>
- Poulter B, Frank D, Ciais P et al (2014) Contribution of semi-arid ecosystems to interannual variability of the global carbon cycle. *Nature* 509:600–603. <https://doi.org/10.1038/nature13376>
- Prince SD, Goward SN (1995) Global primary production: a remote sensing approach. *J Biogeogr* 22:815. <https://doi.org/10.2307/2845983>
- Quaife T, Lewis P, De Kauwe M et al (2008) Assimilating canopy reflectance data into an ecosystem model with an Ensemble Kalman Filter. *Remote Sens Environ* 112:1347. <https://doi.org/10.1016/j.rse.2007.05.020>
- Richardson AD, Anderson RS, Arain MA et al (2012) Terrestrial biosphere models need better representation of vegetation phenology: results from the North American Carbon Program Site Synthesis. *Glob Change Biol* 18:566–584. <https://doi.org/10.1111/j.1365-2486.2011.02562.x>
- Rödig E, Cuntz M, Heinke J et al (2017) Spatial heterogeneity of biomass and forest structure of the Amazon rain forest: linking remote sensing, forest modelling and field inventory. *Glob Ecol Biogeogr* 26:1292–1302. <https://doi.org/10.1111/geb.12639>
- Rödig E, Cuntz M, Rammig A et al (2018) The importance of forest structure for carbon fluxes of the Amazon rainforest. *Environ Res Lett* 13:054013. <https://doi.org/10.1088/1748-9326/aabc61>
- Rodríguez-Veiga P, Saatchi S, Tansey K, Balzter H (2016) Magnitude, spatial distribution and uncertainty of forest biomass stocks in Mexico. *Remote Sens Environ* 183:265–281
- Rogers BM, Soja AJ, Goulden ML, Randerson JT (2015) Influence of tree species on continental differences in boreal fires and climate feedbacks. *Nat Geosci* 8:228–234. <https://doi.org/10.1038/ngeo2352>
- Running SW, Nemani RR, Heinsch FA et al (2004) A continuous satellite-derived measure of global terrestrial primary production. *Bioscience* 54:547. [https://doi.org/10.1641/0006-3568\(2004\)054%5b0547:ACSMOG%5d2.0.CO;2](https://doi.org/10.1641/0006-3568(2004)054%5b0547:ACSMOG%5d2.0.CO;2)
- Saatchi SS, Harris NL, Brown S et al (2011) Benchmark map of forest carbon stocks in tropical regions across three continents. *Proc Natl Acad Sci USA* 108:9899–9904. <https://doi.org/10.1073/pnas.1019576108>
- Santoro M, Beer C, Cartus O et al (2011) Retrieval of growing stock volume in boreal forest using hyper-temporal series of Envisat ASAR ScanSAR backscatter measurements. *Remote Sens Environ* 115:490–507. <https://doi.org/10.1016/j.rse.2010.09.018>
- Santoro M, Beaudoin A, Beer C et al (2015) Forest growing stock volume of the northern hemisphere: spatially explicit estimates for 2010 derived from Envisat ASAR. *Remote Sens Environ* 168:316–334. <https://doi.org/10.1016/j.rse.2015.07.005>
- Scholze M, Buchwitz M, Dorigo W et al (2017) Reviews and syntheses: systematic earth observations for use in terrestrial carbon cycle data assimilation systems. *Biogeosciences* 14:3401–3429
- Schwalm CR, Huntzinger DN, Fisher JB et al (2015) Toward “optimal” integration of terrestrial biosphere models. *Geophys Res Lett* 42:4418–4428. <https://doi.org/10.1002/2015GL064002>
- Shugart HH, Asner GP, Fischer R et al (2015) Computer and remote-sensing infrastructure to enhance large-scale testing of individual-based forest models. *Front Ecol Environ* 13:503–511. <https://doi.org/10.1890/140327>
- Shugart HH, Wang B, Fischer R et al (2018) Gap models and their individual-based relatives in the assessment of the consequences of global change. *Environ Res Lett* 13:033001. <https://doi.org/10.1088/1748-9326/aaaacc>
- Sierra CA, Müller M, Metzler H et al (2017) The muddle of ages, turnover, transit, and residence times in the carbon cycle. *Glob Change Biol* 23:1763–1773. <https://doi.org/10.1111/gcb.13556>
- Sitch S, Friedlingstein P, Gruber N et al (2015) Recent trends and drivers of regional sources and sinks of carbon dioxide. *Biogeosciences* 12:653–679. <https://doi.org/10.5194/bg-12-653-2015>
- Slevin D, Tett SFB, Exbrayat J-F et al (2017) Global evaluation of gross primary productivity in the JULES land surface model v3.4.1. *Geosci Model Dev* 10:2651–2670. <https://doi.org/10.5194/gmd-10-2651-2017>
- Smallman TL, Exbrayat J-F, Mencuccini M et al (2017) Assimilation of repeated woody biomass observations constrains decadal ecosystem carbon cycle uncertainty in aggrading forests. *J Geophys Res Biogeosci* 122:528–545. <https://doi.org/10.1002/2016JG003520>
- Stavros EN, Schimel D, Pavlick R et al (2017) ISS observations offer insights into plant function. *Nat Ecol Evol* 1:0194. <https://doi.org/10.1038/s41559-017-0194>
- Stöckli R, Rutishauser T, Baker I et al (2011) A global reanalysis of vegetation phenology. *J Geophys Res* 116:G03020. <https://doi.org/10.1029/2010JG001545>




- Sun Y, Frankenberg C, Jung M et al (2018) Overview of solar-induced chlorophyll fluorescence (SIF) from the orbiting carbon observatory-2: retrieval, cross-mission comparison, and global monitoring for GPP. *Remote Sens Environ* 209:808–823. <https://doi.org/10.1016/j.rse.2018.02.016>
- Taylor KE, Stouffer RJ, Meehl GA (2012) An overview of CMIP5 and the experiment design. *Bull Am Meteorol Soc* 93:485–498. <https://doi.org/10.1175/BAMS-D-11-00094.1>
- Thum T, Zaehle S, Köhler P et al (2017) Modelling sun-induced fluorescence and photosynthesis with a land surface model at local and regional scales in northern Europe. *Biogeosciences* 14:1969–1987. <https://doi.org/10.5194/bg-14-1969-2017>
- Thurner M, Beer C, Santoro M et al (2014) Carbon stock and density of northern boreal and temperate forests. *Glob Ecol Biogeogr* 23:297–310. <https://doi.org/10.1111/geb.12125>
- Thurner M, Beer C, Carvalhais N et al (2016) Large-scale variation in boreal and temperate forest carbon turnover rate related to climate. *Geophys Res Lett* 43:4576–4585. <https://doi.org/10.1002/2016GL068794>
- Thurner M, Beer C, Ciais P et al (2017) Evaluation of climate-related carbon turnover processes in global vegetation models for boreal and temperate forests. *Glob Change Biol* 23:3076–3091. <https://doi.org/10.1111/gcb.13660>
- Tramontana G, Jung M, Schwalm CR et al (2016) Predicting carbon dioxide and energy fluxes across global FLUXNET sites with regression algorithms. *Biogeosciences* 13:4291–4313. <https://doi.org/10.5194/bg-13-4291-2016>
- van der Tol C, Verhoef W, Rosema A (2009) A model for chlorophyll fluorescence and photosynthesis at leaf scale. *Agric For Meteorol* 149:96. <https://doi.org/10.1016/j.agrformet.2008.07.007>
- van der Werf GR, Morton DC, DeFries RS et al (2009) CO<sub>2</sub> emissions from forest loss. *Nat Geosci* 2:737–738. <https://doi.org/10.1038/ngeo671>
- van der Werf GR, Randerson JT, Giglio L et al (2010) Global fire emissions and the contribution of deforestation, savanna, forest, agricultural, and peat fires (1997–2009). *Atmos Chem Phys* 10:11707–11735. <https://doi.org/10.5194/acp-10-11707-2010>
- Waigl CF, Stuefer M, Prakash A, Ichoku C (2017) Detecting high and low-intensity fires in Alaska using VIIRS I-band data: an improved operational approach for high latitudes. *Remote Sens Environ* 199:389–400. <https://doi.org/10.1016/j.rse.2017.07.003>
- Warszawski L, Frieler K, Huber V et al (2014) The inter-sectoral impact model intercomparison project (ISI-MIP): project framework. *Proc Natl Acad Sci USA* 111:3228–3232. <https://doi.org/10.1073/pnas.1312330110>
- Williams M, Schwarz PA, Law BE et al (2005) An improved analysis of forest carbon dynamics using data assimilation. *Glob Change Biol* 11:89–105. <https://doi.org/10.1111/j.1365-2486.2004.00891.x>
- Williams M, Richardson AD, Reichstein M et al (2009) Improving land surface models with FLUXNET data. *Biogeosciences* 6:1341–1359. <https://doi.org/10.5194/bg-6-1341-2009>
- Wood JD, Griffis TJ, Baker JM et al (2017) Multiscale analyses of solar-induced fluorescence and gross primary production. *Geophys Res Lett* 53:785–818. <https://doi.org/10.1002/2016gl070775>
- Worden JR, Bloom AA, Pandey S et al (2017a) Reduced biomass burning emissions reconcile conflicting estimates of the post-2006 atmospheric methane budget. *Nat Commun* 8:2227. <https://doi.org/10.1038/s41467-017-02246-0>
- Worden JR, Doran G, Kulawik S et al (2017b) Evaluation and attribution of OCO-2 XCO<sub>2</sub> uncertainties. *Atmos Meas Tech* 10:2759–2771. <https://doi.org/10.5194/amt-10-2759-2017>
- Xu L, Saatchi SS, Shapiro A et al (2017) Spatial distribution of carbon stored in forests of the Democratic Republic of Congo. *Sci Rep* 7:15030. <https://doi.org/10.1038/s41598-017-15050-z>
- Yang X, Tang J, Mustard JF et al (2015) Solar-induced chlorophyll fluorescence that correlates with canopy photosynthesis on diurnal and seasonal scales in a temperate deciduous forest. *Geophys Res Lett* 42:2977–2987. <https://doi.org/10.1002/2015GL063201>
- Yang H, Yang X, Zhang Y et al (2017) Chlorophyll fluorescence tracks seasonal variations of photosynthesis from leaf to canopy in a temperate forest. *Glob Change Biol* 23:2874–2886. <https://doi.org/10.1111/gcb.13590>
- Yokota T, Yoshida Y, Eguchi N et al (2009) Global concentrations of CO<sub>2</sub> and CH<sub>4</sub> retrieved from GOSAT: first preliminary results. *SOLA* 5:160–163. <https://doi.org/10.2151/sola.2009-041>
- Zhang Y, Guanter L, Berry JA et al (2014) Estimation of vegetation photosynthetic capacity from space-based measurements of chlorophyll fluorescence for terrestrial biosphere models. *Glob Change Biol* 20:3727–3742. <https://doi.org/10.1111/gcb.12664>
- Zhang Y, Xiao X, Jin C et al (2016) Consistency between sun-induced chlorophyll fluorescence and gross primary production of vegetation in North America. *Remote Sens Environ* 183:154–169. <https://doi.org/10.1016/j.rse.2016.05.015>



- Zhao M, Running SW (2010) Drought-induced reduction in global. *Science* (80) 329:940–943. <https://doi.org/10.1126/science.1192666>
- Zhu Z, Bi J, Pan Y et al (2013) Global data sets of vegetation leaf area index (LAI)3g and fraction of photo-synthetically active radiation (FPAR)3g derived from global inventory modeling and mapping studies (GIMMS) normalized difference vegetation index (NDVI3G) for the period 1981 to 2011. *Remote Sens* 5:927–948. <https://doi.org/10.3390/rs5020927>
- Zhu Z, Piao S, Myneni RB et al (2016) Greening of the earth and its drivers. *Nat Clim Change* 6:791–795. <https://doi.org/10.1038/nclimate3004>
- Zwally HJ, Schutz B, Abdalati W et al (2002) ICESat's laser measurements of polar ice, atmosphere, ocean, and land. *J Geodyn* 34:405–445. [https://doi.org/10.1016/S0264-3707\(02\)00042-X](https://doi.org/10.1016/S0264-3707(02)00042-X)
- Ziehn T, Scholze M, Knorr W (2012) On the capability of Monte Carlo and adjoint inversion techniques to derive posterior parameter uncertainties in terrestrial ecosystem models. *Glob Biogeochem Cycles* <https://doi.org/10.1029/2011GB004185>

**Publisher's Note** Springer Nature remains neutral with regard to jurisdictional claims in published maps and institutional affiliations.

## Affiliations

**Jean-François Exbrayat<sup>1</sup>**  · **A. Anthony Bloom<sup>2</sup>** · **Nuno Carvalhais<sup>3,6</sup>** · **Rico Fischer<sup>4</sup>** · **Andreas Huth<sup>4,7,8</sup>** · **Natasha MacBean<sup>5</sup>** · **Mathew Williams<sup>1</sup>**

<sup>1</sup> National Centre for Earth Observation and School of GeoSciences, University of Edinburgh, Crew Building, Alexander Crum Brown Road, Edinburgh EH9 3FF, UK

<sup>2</sup> Jet Propulsion Laboratory, California Institute of Technology, Pasadena, CA 91109, USA

<sup>3</sup> Max Planck Institute for Biogeochemistry, Department Biogeochemical Integration, Hans-Knoell-Str. 10, 07745 Jena, Germany

<sup>4</sup> Helmholtz Centre for Environmental Research – UFZ, Department of Ecological Modelling, Permoserstraße 15, 04318 Leipzig, Germany

<sup>5</sup> Department of Geography, Indiana University, 701 E Kirkwood Avenue, Bloomington, IN 47405, USA

<sup>6</sup> CENSE, Departamento de Ciências e Engenharia do Ambiente, Faculdade de Ciências e Tecnologia, Universidade NOVA de Lisboa, Campus de Caparica, 2829-516 Caparica, Portugal

<sup>7</sup> Institute of Environmental Systems Research, University of Osnabrück, Barbarastraße 12, 49076 Osnabrück, Germany

<sup>8</sup> German Centre for Integrative Biodiversity Research (iDiv) Halle-Jena-Leipzig, Deutscher Platz 5e, 04103 Leipzig, Germany